

C β -Selective Aldol Addition of D-Threonine Aldolase by Spatial Constraint of Aldehyde Binding

Sung-Hyun Park,[#] Hogyun Seo,[#] Jihye Seok, Haseong Kim, Kil Koang Kwon, Soo-Jin Yeom,^{*} Seung-Goo Lee,^{*} and Kyung-Jin Kim^{*}



Cite This: *ACS Catal.* 2021, 11, 6892–6899



Read Online

ACCESS |



Metrics & More



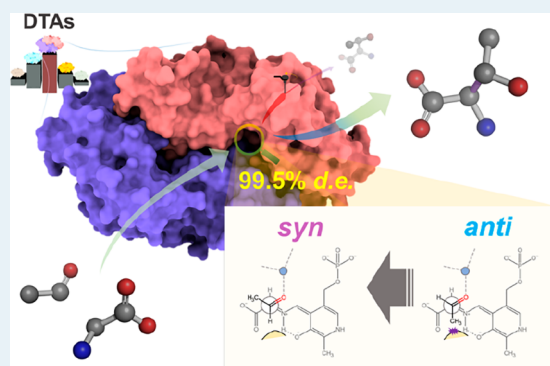
Article Recommendations



Supporting Information

ABSTRACT: D-Threonine aldolase (DTA) is a useful biocatalyst that reversibly converts glycine and aldehyde to β -hydroxy- α -D-amino acid. However, low activity and poor diastereoselectivity limit its applications. Here we report DTA from *Filomicrobium marinum* (*FmDTA*) that shows much higher activity and C β -stereoselectivity in D-threonine production compared with those of other known DTAs. We determine the *FmDTA* structure at a 2.2 Å resolution and propose a DTA catalytic mechanism with a kernel of the Lys49 inner proton sink and metal ion in the aldol reaction cycle. The enzyme is rationally engineered to have high C β -stereoselectivity based on spatial constraint at the *anti*-specific aldehyde position in the mechanism, and the rational strategy is further applied to other DTAs for *syn*-production. The final *FmDTA*^{G179A/S312A} variant exhibits a near-perfect 99.5% de value for D-threonine and maintains the de value above 93% even under kinetically unfavorable conditions. This study demonstrates how a detailed understanding of the reaction mechanism can be used for rational protein engineering.

KEYWORDS: D-threonine aldolase, stereoselectivity, β -hydroxy- α -amino acid, catalytic mechanism, protein engineering



INTRODUCTION

Aldolases transform the carbon skeleton into a larger molecule by forming a carbon and carbon bond (C–C) and play critical roles in organic matter cycling in nature. The reaction can be used to produce and reconstruct the building blocks of many high-value compounds under green conditions.^{1,2} In particular, the aldol addition reaction enabled by enzymes is of interest in chemical industries due to the chiral-selectivity of the biocatalyst.^{3,4}

Pyridoxal-5'-phosphate (PLP)-dependent threonine aldolases (TAs) catalyze the C–C bond formation reaction between the α -carbon ($C\alpha$) of glycine and acetaldehyde. The catalytic promiscuity of aldehyde selection has made the enzymes an important method for the synthesis of β -hydroxy- α -amino acids, which provide a versatile platform for various high-value compounds, such as active pharmaceutical ingredients, antibiotics, or agrochemical building blocks.^{5–9} However, the insufficient diastereoselectivity of TAs at the C β restricts the biocatalyst-based method for β -hydroxy- α -amino acids.^{2,10–15}

A number of studies have attempted to control C β -specificity by changing reaction conditions to favor kinetic or thermodynamic control/influence, but altering the regulated conditions inevitably limited the performance and usage of TAs.^{11–13} Thus, protein engineering approaches have been carried out to overcome the C β -stereoselectivity problem of

low-specificity L-threonine aldolase (LTA, EC 4.1.2.48).^{10,16–19} However, there have been no engineering efforts exerted on the D-threonine aldolase (DTA, EC 4.1.2.42). Unlike L-threonine or L-allo-threonine aldolase (EC 4.1.2.5 or 4.1.2.49),²⁰ there are no C β -specific DTA enzymes known. Although the crystal structure of the DTA from *Alcaligenes xylosoxidans* (*AxDTA*) has been reported,²¹ the underlying principle of the low C β -stereospecificity of DTAs has still not been elucidated. Herein, we provide a study on rational design protein engineering to tailor the C β -selectivity of DTAs, which comprises the multidisciplinary works of enzyme identification, structural analysis, and catalytic mechanisms.

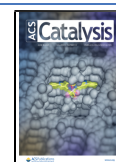
RESULTS

Identification of *FmDTA*. To identify an enzyme with high aldol activity and C β -selectivity, we performed a phylogenetic analysis of DTAs and selected four DTA candidates from *Achromobacter insolitus* (*AiDTA*), *Bordetella*

Received: March 24, 2021

Revised: May 14, 2021

Published: May 28, 2021



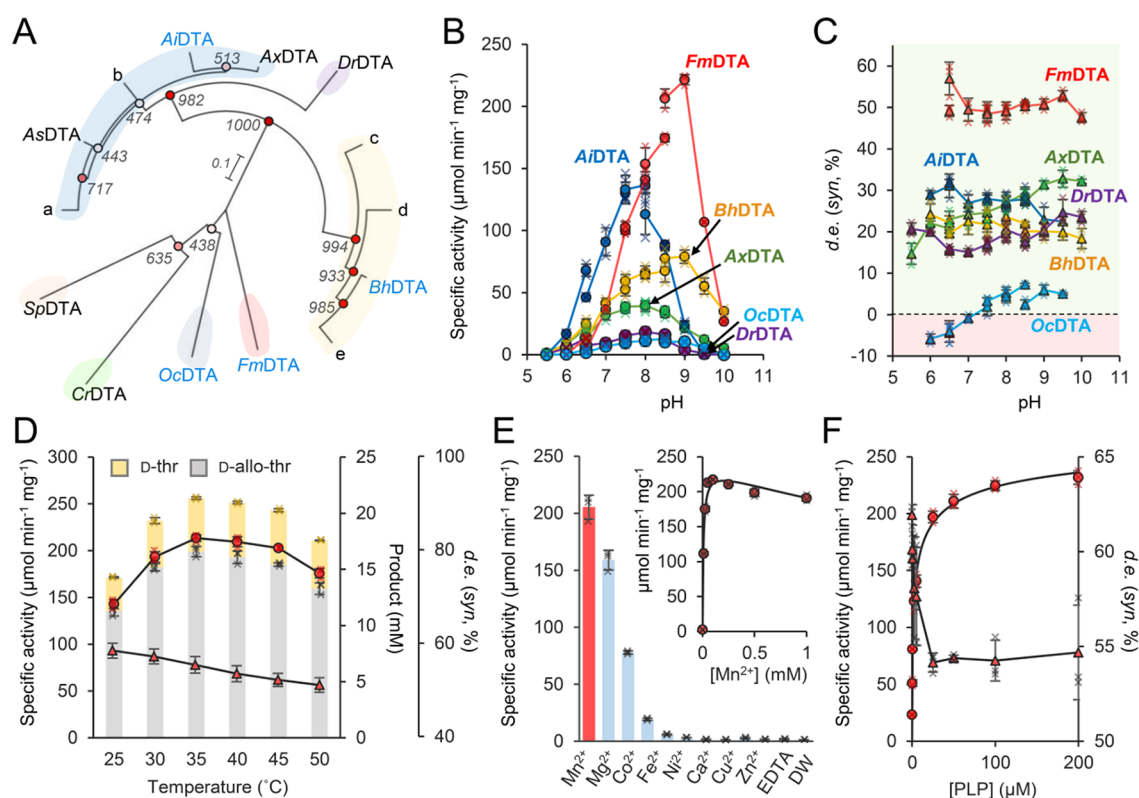


Figure 1. Identification of *FmDTA*. (A) The unrooted maximum likelihood phylogenetic tree of DTAs. The known DTAs and the newly selected DTAs in this study are labeled with black and blue colors, respectively. The clades are distinguished with different background colors. The bootstrap values in 1000 replication are shown at the branching edges and also expressed with red circles with lightness. The nodes of the alphabet indicate its sequence accession code in the NCBI database: (a) WP_050728312, (b) WP_183007039, (c) WP_081695032, (d) WP_005017435, and (e) WP_164855593. (B–F) All of the reactions were performed with 100 mM glycine, 100 mM acetaldehyde, and 50 mM buffer conditions for 10 min. (B) Specific activities of DTAs. Standard deviations are shown as bars ($n = 3$). (C) The diastereomeric excess achieved by the DTAs. Standard deviations are shown as bars ($n = 3$). (D) Temperature effect on *FmDTA* activity. The total product concentration is shown with the sum of D-threonine and D-allo-threonine concentration. Standard deviations are shown as bars ($n = 3$). (E) Metal ion preference of *FmDTA*. Standard deviations are shown as bars ($n = 3$). (F) The concentration-dependent data were fitted with the modified Briggs–Haldane equation. (F) The effect of PLP concentration on enzyme activity (circles) and de value for selectivity (triangles). Standard deviations are shown as bars ($n = 3$). The activity data were fitted with the Hill equation.

hinzii (*BhDTA*), *Oligotropha carboxidovorans* (*OcDTA*), and *Filomicrobium marinum* (*FmDTA*), which show a low phylogram relationship (Figure 1A, Figure S1, Tables S1–2). We then measured the specific aldol activities of the selected enzymes and the aldol activities with those of *AxDTA*, which is the most extensively studied enzyme among DTAs, using a pH range of 5.5–10.0.^{11,13,22–25} Considering that acetaldehyde is the basic form of the aldehyde substrate that exacerbates the selectivity problem of DTA,^{22–25} we used acetaldehyde as a substrate. Although all DTAs showed an optimal pH in the alkaline pH ranging from 7.5 to 9.0, three DTAs, such as *BhDTA*, *AiDTA*, and *FmDTA*, exhibited higher activities than those of *AxDTA* (Figure 1B). In particular, *FmDTA* showed 4.7-fold higher aldol activity than that of *AxDTA* under optimal pH conditions (Figure 1B). Moreover, the enzyme exhibited a superb de (46–51%) for D-threonine, depending on the pH conditions, compared with that of other DTAs with up to 30% de value (*syn*) (Figure 1C). We then investigated the detailed enzyme characteristics of *FmDTA*. When we measured the enzyme activity at various temperatures, *FmDTA* showed a maximum activity at 35 °C and maintained its specific activity around 150 $\mu\text{mol min}^{-1} \text{mg}^{-1}$ over the broad temperature range from 25 to 50 °C (Figure 1D). *FmDTA* showed a clear dependency on divalent metal ions, such as

Mn^{2+} , Mg^{2+} , Co^{2+} , and Fe^{2+} , and the highest activity was observed for Mn^{2+} (Figure 1E). *FmDTA* also required approximately 100 μM extrinsic PLP for the maximized activity; however, the enzyme showed higher *syn*-selectivity under a lower PLP concentration (Figure 1F).

Crystal Structure of *FmDTA*. Although the diastereoselectivity of *FmDTA* was relatively higher than that of other DTAs we tested, the product still has a racemic problem when using the DTA-based method. We then determined the crystal structure of *FmDTA* to elucidate the molecular mechanism of the enzyme and to provide a rational strategy increasing the $C\beta$ -specificity. The crystals belonged to the $P2_12_12$ space group with unit cell dimensions of $a = 71.0$, $b = 178.1$, and $c = 65.5$ (Table S3). The asymmetric unit contained a dimeric form of *FmDTA*, and the size-exclusion chromatographic data also revealed that the protein functions as a dimer in solution (Figure S2). The structure of *FmDTA* exhibits a canonical alanine racemase fold: the $(\alpha/\beta)_8$ -barrel-like domain was decorated with a subsidiary part (β -decoration) at the N-, C-termini, which comprises an α -helix, a 3_{10} -helix, and eight continuously connected tangled β -strands (Figure S3). Although the dimeric structure of *FmDTA* exhibits a root-mean-square deviation value of 0.78 with the $C\alpha$ -coordinates of *AxDTA*, the spatial coordinates are somewhat different,

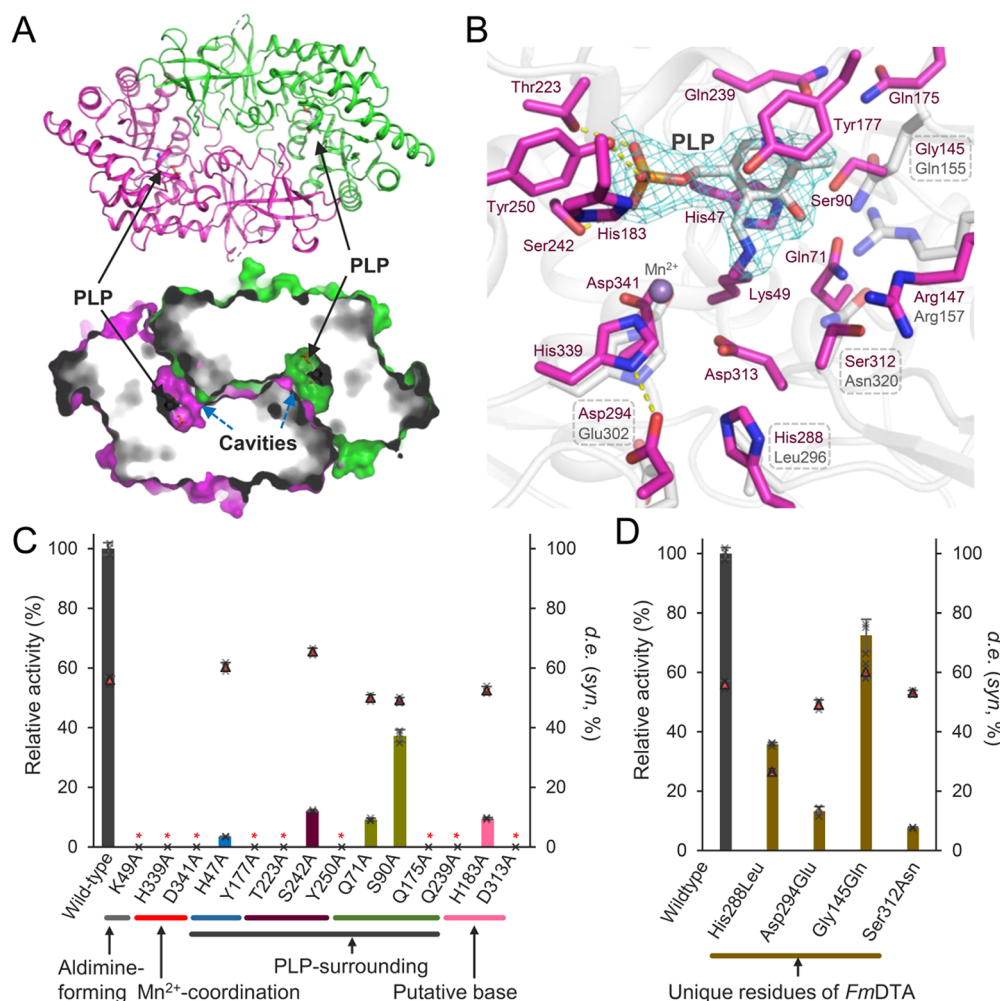


Figure 2. Structure and key residues of *FmDTA*. (A) Overall dimeric structure of *FmDTA*. The structure of *FmDTA* is shown as cartoon (upper) and surface (lower) models. (B) Active site of *FmDTA*. The key residues at the active site are shown as magenta sticks and superposed with the *AxDTA* cartoon model with a Mn^{2+} (PDB code 4V15). Key residues of *FmDTA* and *AxDTA* are distinguished with colors of magenta and gray, respectively. Hydrogen bonds and coordination interaction are indicated by yellow dotted lines. The simulated-annealing composite OMIT map for PLP contoured at 1.0σ is shown with the cyan mesh. (C, D) Site-directed mutagenesis. The enzyme activities of the variants were measured at the pH 9.0 condition with 100 mM glycine, 100 mM acetaldehyde, 0.1 mM PLP, and 0.1 mM $MnCl_2$, and 0.015 mg mL⁻¹ enzyme. The relative activity is shown with bar graph, and the corresponding d_e value is shown with triangles. Standard deviations are shown as bars ($n = 3$).

which is likely attributed to the differences in their enzymatic characteristics (Figure S4).

Lys49-PLP internal aldimine is located at the active site cavity that forms at the dimerization interface (Figure 2A,B). The PLP coenzyme is surrounded by residues that are presumed to be involved in enzyme catalysis and/or substrate/metal ion binding (Figure 2B). The pyridoxal moiety of PLP is interposed in the ring structures of Tyr177 and His47, and the residues of Gln71 and Ser90 are also in contact with the moiety (Figure 2B). The phosphate moiety forms hydrogen bonds with the hydroxyl groups of Thr223, Ser242, and Tyr250 (Figure 2B). His339 and Asp341 are highly conserved residues for the coordination of Mn^{2+} in *AxDTA*, and His183 is located close to the position of the metal ion (Figure 2B).²¹ The residue involvement in enzyme activity was assessed by alanine-scanning site-directed mutagenesis, and the replacements resulted in complete loss or a dramatic decrease of aldol addition activities (Figure 2C). Interestingly, the Gln239 residue is located in the vicinity of the pyridine nitrogen of PLP (N1-PLP) with a distance of 3.1 Å by providing a polar carboxamide moiety to the nitrogen atom

(Figure 2C). However, alanine racemases, which share a fold that is similar to DTAs but does not adopt a quinonoid formation during enzyme catalysis, have an arginine residue at the corresponding position of Gln239 of *FmDTA*.^{26,27} Structural comparisons with other PLP-dependent enzymes at the corresponding position implied that Gln239 is related with the protonation state of N1-PLP and quinonoid intermediate formation (Figure S5, Note S1). The complete loss of activity of the *FmDTA*^{Q239A} variant confirmed that the Gln239 residue is heavily involved in enzyme catalysis (Figure 2C). Moreover, we found several unique residues in the second layer of the PLP-binding site of *FmDTA*, such as Gly145, His288, Asp294, and Ser312 (Figure 2B). Substitutions of these residues with the corresponding residues of *AxDTA* showed a 25–80% decrease in activity (Figure 2D), which indicates that these unique residues might contribute to the higher catalytic potential of *FmDTA* rather than that of *AxDTA*.

Catalytic Mechanism of *FmDTA* with an Inner Proton Sink. Comprehensive understanding of the catalytic mechanisms of DTAs is crucial for determining $C\beta$ -stereospecificity,

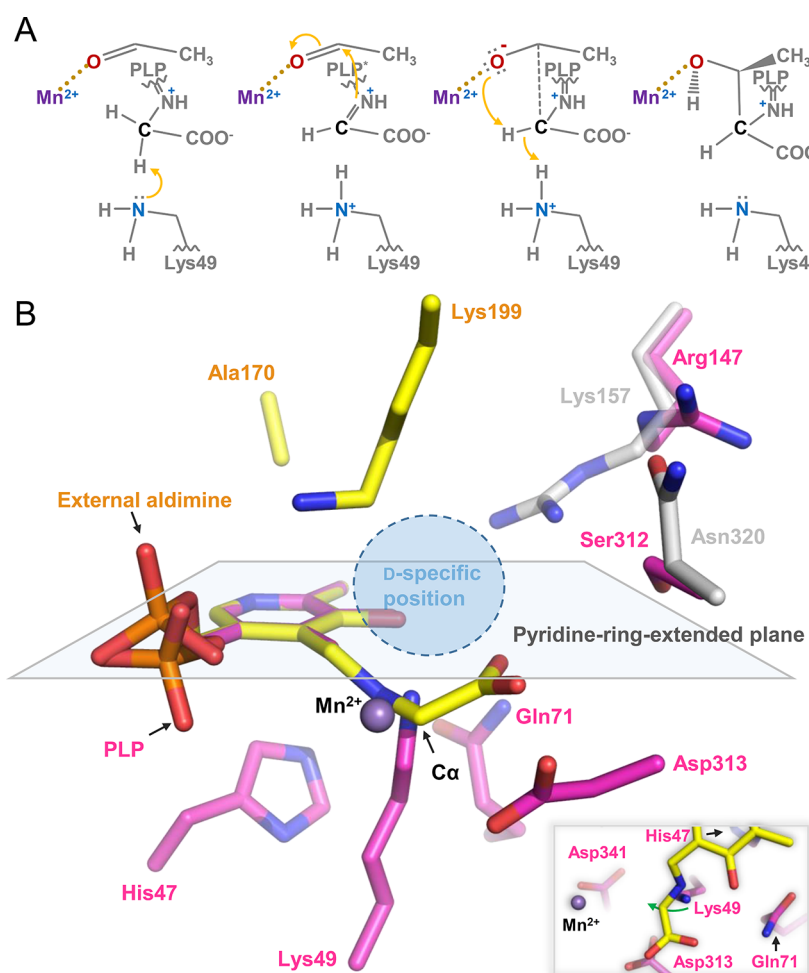


Figure 3. Catalytic residues and pyridine-ring-extended plane in *FmDTA*. (A) The critical steps in the proposed mechanism showing circular electron-relay by the proton sink. PLP and PLP* denote the PLP structure with an amine group and its quinonoid form, respectively. The whole mechanism is described in Scheme S1. (B) Mirror-like catalytic site superposition between *FmDTA* and an LTA from *Aeromonas jandaei* (PDB code 3WGB). The residues and the glycine-PLP external aldimine in the LTA are shown as yellow sticks. Lys49 and its surrounding residues in *FmDTA* are shown with magenta sticks. The pyridine-ring-extended plane and the possible D-specific position of aldehyde are shown and labeled. Two residues of *FmDTA* and *AxDTA* close to the aldehyde position are shown with magenta and gray sticks, respectively. The Mn^{2+} ion is prepared from the structure of *AxDTA*. The small figure is a top view of the large figure, and the green arrow indicates the possible position of the free Lys49.

because the positional relationship between the aldehyde and glycine substrates determines the stereospecificity of the enzyme. A previous study on *AxDTA* suggested the retroaldol reaction (reverse reaction) mechanism of DTA, where His193 drives water-mediated deprotonation of the $C\beta$ -hydroxyl group of a substrate.^{15,21} The mechanism is quite similar to a mechanism found in LTAs and the redesigned alanine racemases, by using the histidine residue as a protonation and deprotonation mediator.^{18,28} The proposed mechanism, however, is in conflict with our mutational study where the *FmDTA*^{H183A} variant showed a detectable activity (Figure 2C). Production of a significant amount of D-threonine and D-allo-threonine with a higher concentration of the variant indicates that the histidine residue does not participate directly in enzyme catalysis (Figure S6). In fact, His183 is involved in the binding of PLP by stabilizing the crucial Tyr250 residue (Figure S7), which seems to explain the reduced activity of the variant. Moreover, considering the pK_a of biprotonated histidine,^{29,30} the proton-received histidine may not be stable at the optimum pH values for DTA (Figure 1B).

It is of interest that, besides His183, there is no acidic protein residue that can give a proton to the oxygen of aldehyde within the active site (Figure 2B). We thus assumed a mechanism that excludes the external proton-withdrawing residue, reassessing the functions of the metal ion and Lys49 (Figure 3A, Scheme S1). The lysine-mediated $C\alpha$ -deprotonation is a reaction trigger mechanism commonly found in the PLP-dependent enzymes, such as aminotransferases, tyrosine phenol-lyases, and *O*-phospho-L-seryl-tRNA^{Sec}:L-selenocystein-tRNA synthase (Note S1).^{31–33} In the newly proposed mechanism, proton abstraction at the $C\alpha$ by Lys49 inner proton sink initiates enzyme catalysis (Figure 3A, Scheme S1). When the resulting carbanion attacks aldehyde, the divalent metal ion stabilizes the oxyanion state of the $C\beta$ -oxygen (Figure 3A, Scheme S1), as a rate limiting step.¹¹ Then, $C\beta$ -oxygen receives a proton through a proton-for-proton swap at $C\alpha$, where nucleophilic oxygen attacks the other proton of $C\alpha$ and the carbon regains a proton from the sink (Figure 3A, Scheme S1). An interesting observation is that His47 of *FmDTA* blocks the corresponding position of the aldimine-forming lysine of LTA in a mirror-like catalytic site

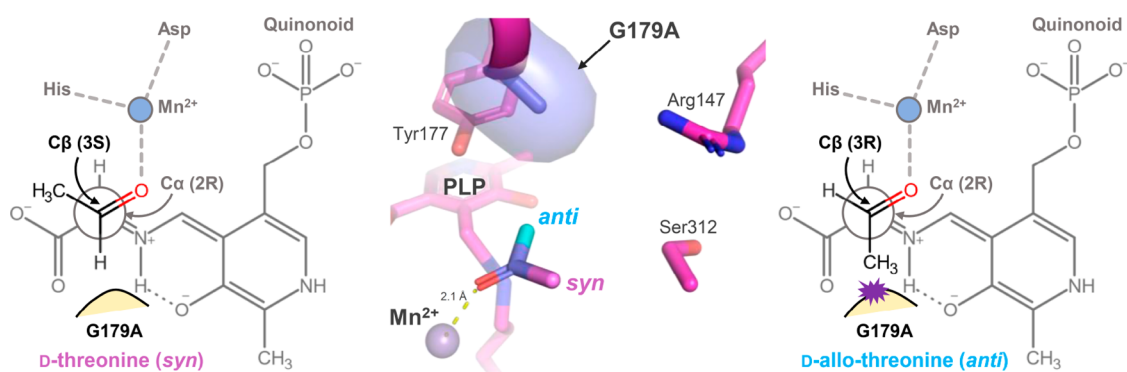


Figure 4. Rational design for the *syn*-specific DTA. The middle panel shows 3D configurations, and the left and right panels show a 2D diagram for the *syn*- and *anti*-positions of acetaldehyde, respectively. The *Fm*DTA residues and the PLP-Lys49 internal aldimine are shown with magenta sticks and labeled. The Mn^{2+} ion is prepared from the structure of *Ax*DTA. G179A and acetaldehyde are prepared by PyMol manipulation and shown as a surface and stick model, respectively. The side-chain of G179A is shown with a block diagram in the two outside panels.

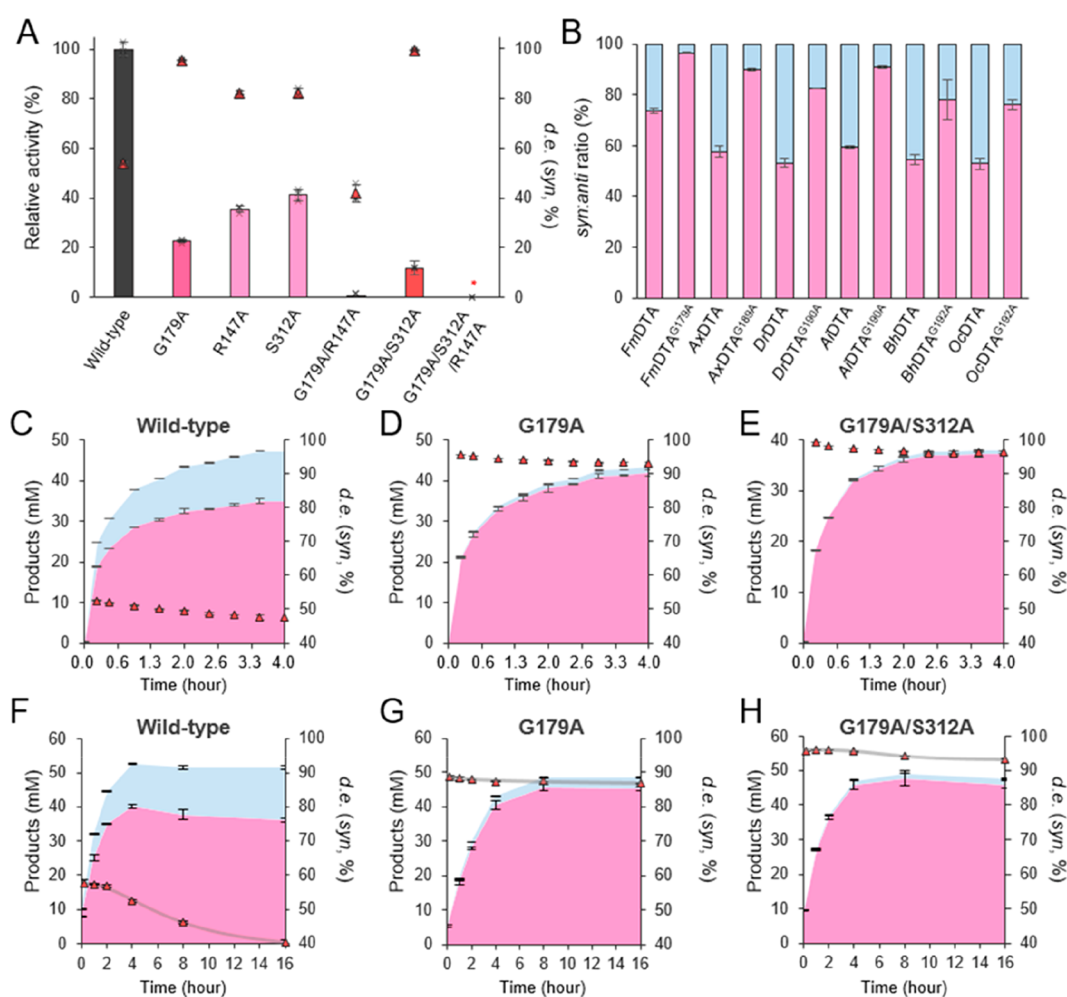


Figure 5. Near-perfect $C\beta$ -stereoselectivity of the *Fm*DTA variants. (A) Relative activities and d_e values (*syn*) of the engineered enzymes. Standard deviations are shown as bars ($n = 3$). (B) Rational design application to other DTAs. Standard deviations are shown with bars ($n = 3$). (C–E) Changes of accumulated products and d_e values by the *Fm*DTA variants. Pink and blue areas indicate concentrations of *D*-threonine and *D*-allo-threonine, respectively. The reactions were performed with 500 mM glycine, 100 mM acetaldehyde, 0.1 mM PLP, 0.1 mM MnCl_2 , and enzyme concentrations of 0.01, 0.05, or 0.09 mg mL^{-1} , respectively. Standard deviations are shown ($n = 3$). (F–H) Changes of accumulated products and d_e values by the *Fm*DTA variants over the long period of time. The reactions were performed under the same conditions as above, but the temperature was set at 15 °C in view of the volatility of acetaldehyde. The decreased d_e values are fitted to the logistic equation, and the graph is shown with a gray line. Standard deviations are shown ($n = 3$).

superposition, indicating that DTA has a different mechanism compared to those of LTAs (Figure 3B), whereupon when

external aldimine is formed, the free and uncharged lysine may be positioned to a limited space located under the pyridine-

ring-extended plane close to the potential position of $C\alpha$ (Figure 3B). Asp313 seems to aid the proton abstraction by the sink, and complete activity abolishment of the $FmDTA^{D313A}$ variant and restriction of Lys49 positioning strongly support the proton sink concept (Figures 2C and 3B). This proposed mechanism explains the metal-dependency of DTA and the flow of protons that transform aldehyde into the $C\beta$ -hydroxyl group of a product. According to the mechanism, DTA shows a unique enzymatic aldol addition model where only the metal ion and $C\alpha$ with the sink wait for the aldehyde substrate to be trapped, which will be described in the next section.

Rational Engineering for High $C\beta$ -Stereoselectivity.

Our proposed mechanism suggests that the aldehyde substrate is coordinated to a metal ion and is located on the quinonoid structure opposite the inner proton sink (Figure 3). Here, we can expect that the aldehyde substrate in a plane configuration of the formyl group has two possible positions for its R-group, considering the interaction with the quinonoid intermediate. When the R-group is located toward the inner position of the cavity, the *anti*-form of its product (D-allo-threonine) is formed (Figure 4). On the contrary, when the R-group is located toward the outer position of the cavity, the *syn*-form of its product (D-threonine) is formed (Figure 4). We then designed the $FmDTA^{G179A}$ variant based on the rationale that an artificial spatial constraint might hinder the placement of the R-group at the inner position of the cavity (Figure 4). The variant showed a dramatically increased de value of 95.0% for the *syn*-diastereomer, although its activity decreased to 22.6% of the wild-type (Figure 5A). Surprisingly, mutations of the corresponding glycine residue of other DTAs, such as *BhDTA*, *AiDTA*, *OcDTA*, *AxDTA*, and *DrDTA*, to alanine resulted in a dramatic increase of the *syn*-specificity (Figure 5B). These results confirm that the rationale can also be applied to other DTAs, which further supports our proposed reaction mechanism and the aldehyde binding mode of DTA. We also observed the Arg147 and Ser312 residues in the vicinity of the aldehyde binding site (Figures 2B and 3), and mutations of these residues to alanine resulted in one-third of the activity and the increased de value compared with that of the wild-type (Figure 5A), which indicates that these two residues affect the positioning of aldehyde and consequently the stereospecificity determination.

We then attempted to combine the G179A mutation with the R147A and S312A mutations to achieve even higher *syn*-specific variants. Unfortunately, the $FmDTA^{R147A/G179A}$ variant showed a decreased de value, which implies that the R147A mutation abolished the hindrance effect of the G179A mutation (Figure 5A). However, the $FmDTA^{G179A/S312A}$ variant exhibited a much higher de value of 99.5% (Figure 5A). Kinetic analysis of the $FmDTA^{G179A/S312A}$ variant showed a similar level of K_m and a reduced k_{cat} compared with those of the wild-type (Table S4). These results imply that the mutations only affected the direction of the substrate binding without changing its affinity for the substrate, and the position of the bound substrate in the variant is slightly different from that needed for optimal enzyme catalysis. Next, we measured the D-threonine production by the $FmDTA$ variants for 4 h to monitor the changes in the $C\beta$ -stereoselectivity during the extended catalytic processes. We adjusted enzyme quantities to secure an activity level of the wild-type for each of the variants to compare the selectivity while minimizing the kinetic effect. Although the de values (*syn*) decreased in both the

$FmDTA^{G179A}$ and the $FmDTA^{G179A/S312A}$ variants over time, the variants maintained high de values of over 93% and 95%, respectively (Figure 5C–E). Since it is known that one of the drawbacks of TAs is a decrease in the $C\beta$ -stereoselectivity over time,^{11,34} 16 h reactions were conducted to validate that the $FmDTA$ variants maintain the high selectivity without kinetic control. Although the overall conversion was not affected, the wild-type showed a severe decrease of $C\beta$ -stereoselectivity by a 17.4% change in the de value, indicating the kinetic effect in the 4 h reaction (Figure 5F), whereas the $C\beta$ -stereoselectivities of $FmDTA^{G179A}$ and $FmDTA^{G179A/S312A}$ were slightly reduced by 1.8% and 2.4% over the long period of time (Figure 5G,H). The effect of our rational design was further demonstrated with the same experiments using *BhDTA* and the $BhDTA^{G192A}$ variant (Figure S8).

We further tested if the variants can be utilized for other aldehydes. We first measured D-hydroxynorvaline production using a propionaldehyde substrate. For the 16 h reaction, the wild-type produced both *syn*- and *anti*-forms of D-hydroxynorvaline while the peak corresponding to the *anti*-form was negligible in the reactions of $FmDTA^{G179A}$ and $FmDTA^{G179A/S312A}$ (Figure S9). It has been known that DTAs tend to produce *syn*-form products when bulky aromatic substrates are used,^{13,25} which leads us to presume that the *syn*-specific active sites of these variants might prefer benzaldehyde to acetaldehyde as a substrate. When benzaldehyde was used as a substrate, $FmDTA^{WT}$ showed a much higher $C\beta$ -stereoselectivity with a de value (*syn*) of 94.5% than when using acetaldehyde, and the *syn*-specific $FmDTA^{G179A}$ and $FmDTA^{G179A/S312A}$ variants exhibited even higher de values (Table S5). Surprisingly, the catalytic ability of the variants increased 1.40 and 2.61 times compared to that of the wild-type (Table S5). These results are consistent with the presumption that there is a relationship between the mechanistic positioning of aldehyde and the rate of bond formation, further emphasizing that the rationale of the DTA variants is suitable for aldehyde substrates of various sizes.

CONCLUSIONS

In this study, the $FmDTA$ enzyme with high activity and selectivity for D-threonine production was identified. On the basis of the structural and biochemical analyses of $FmDTA$, we proposed a catalytic mechanism of DTA, in which the divalent metal ion plays an important role in the common PLP-dependent mechanism. Comprehensive understanding of the catalytic mechanism of DTA provided us with a strategy for rational protein engineering, by which we achieved the $FmDTA$ variants having near-perfect $C\beta$ -stereoselectivity of a de value of 99.5% for D-threonine. We also demonstrate that the rational design is also applicable to other DTA homologues. This is the first case of asymmetric bioconversion of short-chain aldehydes into β -hydroxy- α -D-amino acids by an unnatural *syn*-specific DTA (Table S6). Furthermore, the $FmDTA^{G179A/S312A}$ variant showed enhanced catalytic activity and $C\beta$ -stereoselectivity against the benzaldehyde substrate. This study on DTAs shows how mechanism-based rational engineering can control enzyme catalysis and can be utilized for β -hydroxy- α -D-amino acid conversion.

ASSOCIATED CONTENT

Supporting Information

The Supporting Information is available free of charge at <https://pubs.acs.org/doi/10.1021/acscatal.1c01348>.

Methods and supporting note (Note S1) and additional results presented in tables (Tables S1–S6), figures (Figures S1–S10), and scheme (Scheme S1) (PDF)

AUTHOR INFORMATION

Corresponding Authors

Kyung-Jin Kim – School of Life Sciences, BK21 FOUR KNU Creative BioResearch Group, KNU Institute for Microorganisms, Kyungpook National University, Daegu 41566, Republic of Korea; orcid.org/0000-0002-0375-2561; Phone: +82-53-950-5377; Email: kkim@knu.ac.kr

Seung-Goo Lee – Synthetic Biology and Bioengineering Research Center, Korea Institute of Bioscience and Biotechnology (KRIBB), Daejeon 34141, Republic of Korea; Department of Biosystems and Bioengineering, KRIBB School, University of Science and Technology (UST), Daejeon 34113, Republic of Korea; orcid.org/0000-0003-4539-9812; Phone: +82-42-860-4373; Email: sglee@kribb.re.kr

Soo-Jin Yeom – School of Biological Sciences and Technology, Chonnam National University, Gwangju 61186, Republic of Korea; Phone: +82-62-530-1911; Email: soojin258@chonnam.ac.kr

Authors

Sung-Hyun Park – Synthetic Biology and Bioengineering Research Center, Korea Institute of Bioscience and Biotechnology (KRIBB), Daejeon 34141, Republic of Korea; Department of Biosystems and Bioengineering, KRIBB School, University of Science and Technology (UST), Daejeon 34113, Republic of Korea

Hogyun Seo – School of Life Sciences, BK21 FOUR KNU Creative BioResearch Group, KNU Institute for Microorganisms, Kyungpook National University, Daegu 41566, Republic of Korea; Pohang Accelerator Laboratory, Pohang University of Science and Technology, Pohang 37673, Republic of Korea

Jihye Seok – School of Life Sciences, BK21 FOUR KNU Creative BioResearch Group, KNU Institute for Microorganisms, Kyungpook National University, Daegu 41566, Republic of Korea

Haseong Kim – Synthetic Biology and Bioengineering Research Center, Korea Institute of Bioscience and Biotechnology (KRIBB), Daejeon 34141, Republic of Korea; Department of Biosystems and Bioengineering, KRIBB School, University of Science and Technology (UST), Daejeon 34113, Republic of Korea

Kil Koang Kwon – Synthetic Biology and Bioengineering Research Center, Korea Institute of Bioscience and Biotechnology (KRIBB), Daejeon 34141, Republic of Korea

Complete contact information is available at: <https://pubs.acs.org/10.1021/acscatal.1c01348>

Author Contributions

*S.-H.P. and H.S. contributed equally to this work. S.-J.Y., S.-G.L., and K.-J.K. conceived the project. S.-H.P., H.K., K.K.K., and S.-J.Y. performed the biochemical experiments. H.S. and J.S. performed the structural determination and the rational design. S.-H.P. and H.S. analyzed the data. S.-G.L., K.-J.K., S.-H.P., H.S., and S.-J.Y. wrote the paper.

Notes

The authors declare the following competing financial interest(s): 10-2019-0131991 and PCT/KR2020/01429.

The structure of *Fm*DTA is deposited in Protein Data Bank with an accession code of 7DIB. The source data underlying Figures 1, 2, and 5a are associated with raw data. The data sets generated and analyzed during the current study are available from the corresponding authors upon request.

ACKNOWLEDGMENTS

This work was supported by the C1 Gas Refinery Program (NRF-2018M3D3A1A01055732 and NRF-2018M3D3A1A01056181) and the Basic Science Research Program (NRF-2020R1A4A1018332) funded by the Ministry of Science and ICT, and the Korea Research Institute of Bioscience and the Biotechnology (KRIBB) Research Initiative Program (KGM5402113).

REFERENCES

- (1) Windle, C. L.; Müller, M.; Nelson, A.; Berry, A. Engineering aldolases as biocatalysts. *Curr. Opin. Chem. Biol.* **2014**, *19*, 25–33.
- (2) de Berardinis, V.; Guérard-Hélaine, C.; Darii, E.; Bastard, K.; Hélaine, V.; Mariage, A.; Petit, J.-L.; Poupard, N.; Sánchez-Moreno, I.; Stam, M.; Gefflaut, T.; Salanoubat, M.; Lemaire, M. Expanding the reaction space of aldolases using hydroxypyruvate as a nucleophilic substrate. *Green Chem.* **2017**, *19*, 519–526.
- (3) Clapés, P.; Fessner, W. D.; Sprenger, G. A.; Samland, A. K. Recent progress in stereoselective synthesis with aldolases. *Curr. Opin. Chem. Biol.* **2010**, *14*, 154–167.
- (4) Wechsler, C.; Meyer, D.; Loschonsky, S.; Funk, L. M.; Neumann, P.; Ficner, R.; Brodhun, F.; Müller, M.; Tittmann, K. Tuning and Switching Enantioselectivity of Asymmetric Carbonylation in an Enzyme through Mutational Analysis of a Single Hot Spot. *ChemBioChem* **2015**, *16*, 2580–2584.
- (5) Schmidt, N. G.; Eger, E.; Kroutil, W. Building bridges: Biocatalytic C–C-bond formation toward multifunctional products. *ACS Catal.* **2016**, *6*, 4286–4311.
- (6) Yoo, C. H.; Yook, J. S.; Lee, W. H.; Lee, J. S.; Lee, J. C.; Lee, C. M.; Lee, T. S. Novel method for producing cefbuperazone intermediate. KR patent 2009, KR 100898103 B1.
- (7) Liu, J. Q.; Odani, M.; Dairi, T.; Itoh, N.; Shimizu, S.; Yamada, H. A new route to L-threo-3-[4-(methylthio)phenylserine], a key intermediate for the synthesis of antibiotics: recombinant low-specificity D-threonine aldolase-catalyzed stereospecific resolution. *Appl. Microbiol. Biotechnol.* **1999**, *51*, 586–591.
- (8) Dücker, N.; Baer, K.; Simon, S.; Gröger, H.; Hummel, W. Threonine aldolases-screening, properties and applications in the synthesis of non-proteinogenic beta-hydroxy-alpha-amino acids. *Appl. Microbiol. Biotechnol.* **2010**, *88*, 409–424.
- (9) Miller, M. J.; Mattingly, P. G.; Morrison, M. A.; Kerwin, J. F., Jr. Synthesis of beta-lactams from substituted hydroxamic acids. *J. Am. Chem. Soc.* **1980**, *102*, 7026–7032.
- (10) Chen, Q.; Chen, X.; Feng, J.; Wu, Q.; Zhu, D.; Ma, Y. Improving and inverting C β -stereoselectivity of threonine aldolase via substrate-binding-guided mutagenesis and a stepwise visual screening. *ACS Catal.* **2019**, *9*, 4462–4469.
- (11) Fesko, K.; Reisinger, C.; Steinreiber, J.; Weber, H.; Schürmann, M.; Griengl, H. Four types of threonine aldolases: similarities and differences in kinetics/thermodynamics. *J. Mol. Catal. B: Enzym.* **2008**, *52*, 19–26.
- (12) Franz, S. E.; Stewart, J. D. Threonine aldolases. *Adv. Appl. Microbiol.* **2014**, *88*, 57–101.
- (13) Kimura, T.; Vassilev, V. P.; Shen, G. J.; Wong, C. H. Enzymatic synthesis of β -hydroxy- α -amino acids based on recombinant D- and L-threonine aldolases. *J. Am. Chem. Soc.* **1997**, *119*, 11734–11742.
- (14) Steinreiber, J.; Fesko, K.; Mayer, C.; Reisinger, C.; Schürmann, M.; Griengl, H. Synthesis of γ -halogenated and long-chain β -hydroxy- α -amino acids and 2-amino-1, 3-diols using threonine aldolases. *Tetrahedron* **2007**, *63*, 8088–8093.

- (15) Fesko, K. Threonine aldolases: perspectives in engineering and screening the enzymes with enhanced substrate and stereo specificities. *Appl. Microbiol. Biotechnol.* **2016**, *100*, 2579–2590.
- (16) Fesko, K. Comparison of L-Threonine Aldolase Variants in the Aldol and Retro-Aldol Reactions. *Front. Bioeng. Biotechnol.* **2019**, *7*, 119.
- (17) Qin, H. M.; Imai, F. L.; Miyakawa, T.; Kataoka, M.; Kitamura, N.; Urano, N.; Mori, K.; Kawabata, H.; Okai, M.; Ohtsuka, J.; Hou, F.; Nagata, K.; Shimizu, S.; Tanokura, M. L-allo-threonine aldolase with an H128Y/S292R mutation from *Aeromonas jandaei* DK-39 reveals the structural basis of changes in substrate stereoselectivity. *Acta Crystallogr., Sect. D: Biol. Crystallogr.* **2014**, *70*, 1695–1703.
- (18) di Salvo, M. L.; Remesh, S. G.; Vivoli, M.; Ghatge, M. S.; Paiardini, A.; D'Aguzzo, S.; Safo, M. K.; Contestabile, R. On the catalytic mechanism and stereospecificity of *Escherichia coli* L-threonine aldolase. *FEBS J.* **2014**, *281*, 129–145.
- (19) Gwon, H. J.; Baik, S. H. Diastereoselective synthesis of L-threo-3,4-dihydroxyphenylserine by low-specific L-threonine aldolase mutants. *Biotechnol. Lett.* **2010**, *32*, 143–149.
- (20) Riario-Sforza, G.; Pagani, R.; Marinello, E. Threonine aldolase and allothreonine aldolase in rat liver. *Eur. J. Biochem.* **1969**, *8*, 88–92.
- (21) Uhl, M. K.; Oberdorfer, G.; Steinkellner, G.; Riegler-Berket, L.; Mink, D.; van Assema, F.; Schürmann, M.; Gruber, K. The crystal structure of D-threonine aldolase from *Alcaligenes xylosoxidans* provides insight into a metal ion assisted PLP-dependent mechanism. *PLoS One* **2015**, *10*, e0124056.
- (22) Hirato, Y.; Tokuhisa, M.; Tanigawa, M.; Ashida, H.; Tanaka, H.; Nishimura, K. Cloning and characterization of d-threonine aldolase from the green alga *Chlamydomonas reinhardtii*. *Phytochemistry* **2017**, *135*, 18–23.
- (23) Liu, J. Q.; Odani, M.; Yasuoka, T.; Dairi, T.; Itoh, N.; Kataoka, M.; Shimizu, S.; Yamada, H. Gene cloning and overproduction of low-specificity D-threonine aldolase from *Alcaligenes xylosoxidans* and its application for production of a key intermediate for parkinsonism drug. *Appl. Microbiol. Biotechnol.* **2000**, *54*, 44–51.
- (24) Kataoka, M.; Ikemi, M.; Morikawa, T.; Miyoshi, T.; Nishi, K.; Wada, M.; Yamada, H.; Shimizu, S. Isolation and characterization of D-threonine aldolase, a pyridoxal-5'-phosphate-dependent enzyme from *Arthrobacter* sp. DK-38. *Eur. J. Biochem.* **1997**, *248*, 385–393.
- (25) Chen, Q.; Chen, X.; Cui, Y.; Ren, J.; Lu, W.; Feng, J.; Wu, Q.; Zhu, D. A new d-threonine aldolase as a promising biocatalyst for highly stereoselective preparation of chiral aromatic β -hydroxy- α -amino acids. *Catal. Sci. Technol.* **2017**, *7*, 5964–5973.
- (26) Major, D. T.; Gao, J. A combined quantum mechanical and molecular mechanical study of the reaction mechanism and alpha-amino acidity in alanine racemase. *J. Am. Chem. Soc.* **2006**, *128*, 16345–16357.
- (27) Chan-Huot, M.; Dos, A.; Zander, R.; Sharif, S.; Tolstoy, P. M.; Compton, S.; Fogle, E.; Toney, M. D.; Shenderovich, I.; Denisov, G. S.; Limbach, H. H. NMR studies of protonation and hydrogen bond states of internal aldimines of pyridoxal 5'-phosphate acid-base in alanine racemase, aspartate aminotransferase, and poly-L-lysine. *J. Am. Chem. Soc.* **2013**, *135*, 18160–18175.
- (28) Seebeck, F. P.; Hilvert, D. Conversion of a PLP-dependent racemase into an aldolase by a single active site mutation. *J. Am. Chem. Soc.* **2003**, *125*, 10158–10159.
- (29) Li, S.; Hong, M. Protonation, tautomerization, and rotameric structure of histidine: a comprehensive study by magic-angle-spinning solid-state NMR. *J. Am. Chem. Soc.* **2011**, *133*, 1534–1544.
- (30) Hansen, A. L.; Kay, L. E. Measurement of histidine pKa values and tautomer populations in invisible protein states. *Proc. Natl. Acad. Sci. U. S. A.* **2014**, *111*, E1705–E1712.
- (31) Kirsch, J. F.; Eichele, G.; Ford, G. C.; Vincent, M. G.; Jansonius, J. N.; Gehring, H.; Christen, P. Mechanism of action of aspartate aminotransferase proposed on the basis of its spatial structure. *J. Mol. Biol.* **1984**, *174*, 497–525.
- (32) Milić, D.; Demidkina, T. V.; Faleev, N. G.; Matković-Calogović, D.; Antson, A. A. Insights into the catalytic mechanism of tyrosine phenol-lyase from X-ray structures of quinonoid intermediates. *J. Biol. Chem.* **2008**, *283*, 29206–29214.
- (33) Palioura, S.; Sherrer, R. L.; Steitz, T. A.; Söll, D.; Simonovic, M. The human SepSecS-tRNA^{Sec} complex reveals the mechanism of selenocysteine formation. *Science* **2009**, *325*, 321–325.
- (34) Xu, L.; Wang, L. C.; Xu, X. Q.; Lin, J. Characteristics of L-threonine transaldolase for asymmetric synthesis of β -hydroxy- α -amino acids. *Catal. Sci. Technol.* **2019**, *9*, 5943–5952.